J Mater Sci (2007) 42:4451–4460
DOI 10.1007/s10853-006-0623-5

Preparation of UV-curable intercalated/exfoliated epoxide/acrylateclays nanocomposite resins

Yu-Young Wang · Tsung-Eong Hsieh

Received: 7 March 2006 / Accepted: 26 June 2006 / Published online: 28 February 2007

Abstract Preparation of UV-curable intercalated/exfoliated epoxide/acrylateclays nanocomposite resins with the addition of specific monomers and solvent *via* the consideration of solubility parameter and chemical reactivity was carried out in this work. Due to the good compatibility with surfactant in acrylateclays and the cationic oligomer in resin matrix, the two additive monomers dispersed uniformly in resin matrix with the swollen acrylateclays before UV curing. As revealed by conversion ratio and DTG analyses, chemical bonds between the two additive monomers, the cationic oligomers and surfactant in acrylateclays were formed during UV irradiation. This, in turn, generated a hybrid acrylate-based/epoxy network and effectively enlarged the lamellae spacing of inorganic clays in nanocomposite resins prepared in this work. The XRD and TEM characterizations revealed that the intercalated clay domains containing exfoliated lamellae about 1 nm in thickness uniformly disperse in polymeric matrix. The nanocomposite resin containing 5 wt.% inorganic filler possessed the physical properties as follows: $T_{d\text{-}5\%}$ = 213 °C, CTE = 80.5 ppm/°C, moisture absorption = 6.12%, average optical transmittance = 83.17%, and adhesion strength on glass substrate = 43.8 kgf/cm^2. The analyses above indicated that the formation of polymeric interpenetrating networks and nanometer-scale exfoliation of clay lamellae not only improve the thermal properties and resistance to moisture permeation, but also retain highly optical transmittance and satisfactory adhesion strength of nanocomposite resins prepared in this work. A better device lifetime property was hence achieved when the nanocomposite resins were applied to the packaging of OLEDs.

Y.-Y. Wang · T.-E. Hsieh (✉)
Department of Materials Science and Engineering, National Chiao Tung University, 1001 Ta Hsueh Road, Hsinchu 30050, Taiwan, R.O.C
e-mail: tehsieh@cc.nctu.edu.tw

Introduction

The UV irradiation is a popular process for the curing of polymeric resins due to the advantages including short curing time, environment-friendly characteristics, application versatility and low temperature/energy demands. In electronic industry, UV-curable resins are widely used as adhesives [1] and encapsulants [2]. For the packaging of organic light-emitting devices (OLEDs), UV-curable sealing resins are specifically desired since the light-emitting materials in devices cannot tolerate high-temperature thermal curing process. Further, the resins must provide excellent hermetic sealing due to the vulnerability to moisture/oxygen attack of light-emitting materials. With the aims to improve the thermal, mechanical, adhesion, and permeation properties of sealing resins for OLED packaging, the synthesis of composite resins *via* photopolymerization becomes an attractive research issue in recent years [3, 4].

Since Decker et al. demonstrated the preparation of UV-curable acrylate-bentonite nanocomposites [5], several UV-curable polymer-clays nanocomposites comprised of various organic matrices such as epoxide, acrylate and urethane have been reported [6–9]. For instance, Keller et al. synthesized the montmorillonites (MMT)/polyurethane-acrylate nanocomposite resin with the intercalation and exfoliation phases [6].

Shemper et al. studied the laponite RD (the ''rapidly dispersing'' gel forming grade in laponite powders)/polyacrylate nanocomposite resin crosslinked by different difunctional agents [7]. The preparation of clays/epoxide, clays/epoxide-vinyl ether, and clays/epoxy-polyacrylate nanocomposite resins was reported by Benfarhi et al. [8]. Our previous study investigated the UV-cured polyacrylate/acrylate-modified MMT (called acrylateclays in this work) nanocomposite resins [10]. This work demonstrated that the methylacrylate groups in self-synthesized λ-shaped surfactants may photochemically react with the acrylate groups in the polyacrylate matrix so that the fabrication of nanocomposite resins with improved properties *via* photo-polymerization is plausible.

Photo-polymerization can be classified either as cationic or radical and each of them possesses certain advantages. For instances, the advantages of cationic-photopolymerized epoxides include high adhesion strength, low oxygen permeability, and small volume change while the advantages of radical-photopolymerized polyacrylate are high photo-polymerization rate and low moisture permeability. In this work, we intend to combine the advantages of above two photo-polymerization processes so that the preparation with evaluating solubility parameters of components and characterizations of UV-curable epoxy/acrylateclays nanocomposite resins were carried out. Since there is no direct bonding between acrylate and epoxide groups, monomers with specific functional groups and appropriate solubility parameters were added to promote the formation of chemical bonds. With suitable amount of monomers added to link the acrylate and epoxy portions as well as the radical photo-initiators, fine dispersion of exfoliated clays could be achieved in polymeric matrix of nanocomposite resins. Substantial improvement of thermal and moisture absorption properties of nanocomposite resins were obtained and a better lifetime property was achieved when such resins were applied to the packaging of OLEDs.

Experimental

Materials

Components of resin matrix for sample preparation, such as 3,4-epoxycyclohexylmethyl 3,4-epoxycyclohexanecarboxylate (the cationic oligomer, O_C), tripropylene glycol, vinyltrimethoxysilane and [4-[(2-hydroxytetradecyl)oxy]phenyl]phenyliodonium hexafluoroantimonate (the photo-initiators for cationic-polymerization) were all purchased from Aldrich Chemical Co. Trimethylopropane triacrylate and glycidyl acrylate ester provided by Sartomer Co. were the additive monomer I (M_I) and monomer II (M_{II}) for the promotion of crosslinking between acrylate-based surfactants and epoxide groups in this study. The photo-initiator for radical-polymerization, 1-hydroxycyclohexylphenyl ketone, was also provided by Sartomer Co. The montmorillonite (MMT) powder (PK802, Pai Kong Ceramic Material Co.) with cationic exchange capacity (CEC) = 95 mEq/100 g was adopted as the inorganic filler in the nanocomposite resins. The preparation methods of resin matrix and acrylateclays have briefly described as follows [10, 11]. A total of 25.4 wt.% tripropylene glycol and 1 wt.% vinyltrimethoxysilane were added with 3,4-epoxycyclohexylmethyl 3,4-epoxycyclohexanecarboxylate. After mixing, 15 wt.% [4-[(2-hydroxytetradecyl)oxy]phenyl]phenyliodonium hexafluoroantimonate was added into above mixture and further stirred to complete the resin matrix preparation. The acrylate-based surfactant was prepared by the reaction of glycidyl acrylate ester and didecylamine (molar ratio = 1:1) in ethanol at 60 °C for 48 h. The product was distilled in a vacuum rotator at $T > 80$ °C to remove the ethanol completely. Acrylateclays were prepared *via* cationic exchange in clay galleries. Before cationic exchange, all pristine clays were dried at 80 °C for 24 h to remove the absorbed H_2O. Above self-synthesized surfactants were first acidified by hydrochloric acid (HCl). The MMT were slowly added in 300 ml distilled water and then stirred for several hours to form suspending solution. The acidified surfactants were added into the aqueous solutions containing pristine MMT in constant proportion and the mixture was stirred for 72–96 h to complete the cationic exchange. The clays after cationic exchange were extracted from above mixture solution by a centrifuge. They were dried in a vacuum oven at 80 °C for 24 h to remove the residual solvent. The characterization of acrylateclays is listed in Table 1 while the chemical structures of O_C, M_I, M_{II} and the acrylate-based surfactant are shown in Fig. 1.

Table 1 TGA data for unmodified and acrylate-modified MMT

	Residual weight (%)		Degree of modification[a] (%)
	Before modification	After modification	
MMT	87.08	57.27	71.36

[a] Degree of modification was calculated according to following formula: [(residual weight before modification) – (residual weight after modification)] ÷ (molar weight of surfactant)} × (1000 ÷ CEC) × 100

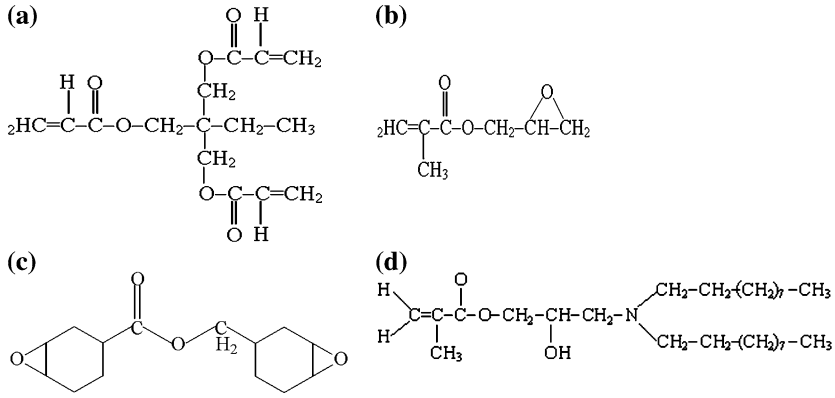

Fig. 1 Molecular structures of: (**a**) monomer I (M_I); (**b**) monomer II (M_{II}), (**c**) cationic oligomer (O_C) and (**d**) the self-synthesized surfactant

Synthesis of epoxide/acrylateclays nanocomposites

The epoxide/acrylateclays nanocomposite resins were prepared by first swelling the acrylateclays by using ultrasonic bath. Anhydrous acetone was chosen as the swelling agent *via* the consideration of solubility parameters and removal/recycling capabilities. Appropriate amount of M_I was then added into the swollen acrylateclays and fully stirred. After removing the acetone from above mixture by heating at 60 °C, M_{II} and the radical photo-initiators were added into acrylateclays/M_I mixture. After mixing, the acrylateclays/M_I/M_{II} was blended with the resin matrix to complete the preparation of nanocomposite resin samples. This procedure was carried out in a yellow-light ambient with wavelength approximately equal to 575 nm. The designated names and compositions of resin samples prepared in this work are listed in Table 2.

Subsequent photo-polymerization was carried out as follows. The resin samples about 10 μm-thick for conversion ratio measurement and 100 μm-thick for thermal, optical and structure characterizations were first coated onto the various substrates such as KBr, teflon and glass, respectively. The specimens were cured in an UV oven (UC-1000, C-Sun) in which the irradiation comes from a 1-kW discharge tube emitting UV light with wavelength ranging from 280 nm to 400 nm to induce the photo-polymerization. After UV exposure, the specimens were post-cured at 80 °C for 1 h.

Table 2 Sample designation and compositions

Sample designation	Monomer I (M_I) (wt.%)	Monomer II (M_{II}) (wt.%)	Acrylateclays (wt.%)	Radical photo-initiators (wt.%)
Resin matrix	–	–	–	–
$S_{ref\text{-}1}$	5.0[a]	–	–	–
$S_{ref\text{-}2}$	5.0[a]	15.0[a]	–	–
$S_{ref\text{-}2\text{-}RPI}$	5.0[a]	15.0[a]	–	3.0[b]
S_1	5.0[a]	15.0[a]	10.0[a]	–
$S_{1\text{-}RPI}$	5.0[a]	15.0[a]	10.0[a]	3.0[b]

[a] The numeric are calculated from the weight ratio of M_I or M_{II} or acrylateclays to resin matrix

[b] The ratio was calculated according to: {(the weight of radical photo-initiators)/[(the total weight of monomers comprising acrylate-based groups) + (the weight of surfactants in acrylateclays)]} × 100

Property characterization

The conversion ratio of resin samples was characterized by a Nicolet Protégé 460 FTIR spectrometer. Measurements of thermal resistance and inorganic content in the resin samples was made using a DuPont 2950 thermogravimetric analyzer (TGA) at a heating rate of 10 °C/min from 30 °C to 800 °C in air ambient. The TGA data were also transformed to plot the differential thermogravimetry (DTG) curves in order to identify the bonding interactions between acrylate-based and epoxy networks in the resin samples. In-plane thermomechanical analysis (TMA) was carried out in a DuPont 2940 TMA with a micro-expansion probe at a heating rate of 10°C/min from 30 °C to 150 °C to identify the coefficient of thermal expansion (CTE) of the samples. The X-ray diffraction (XRD) characterization of nanocomposite resin samples was performed in two different phases: the conventional XRD measurement was performed using a Siemens D5000 X-ray diffractometer with Cu-K_α (λ = 0.1541 nm) radiation, while the grazing incidence X-ray diffraction (GIXRD) measurement was carried out at end station BL17B1 of National Synchrotron Radiation Research Center (NSRRC) Taiwan, with X-ray wavelength set to 0.1240 nm and incident angle fixed at 0.25° to increase X-ray path length. Micro-structures of the samples were examined by a Philips TECNAI G2 transmission electron microscope (TEM)

operating at 200 kV. Moisture absorption was evaluated as follows. Each sample was first immersed in DI water at room temperature for 24 h and then weighed the absorbed moisture after completely drying the residual water on the surface of specimens. Adhesion strength of resin samples on glass substrate was measured in accordance with ASTM D-3528 standard. The transmittance of resin films was characterized by HP 843 UV-visible spectrometer with scanning wavelength ranging from 190 nm to 1200 nm.

The OLEDs consisting of sequent layers of cathode electrode, light-emitting materials and anode electrode were fabricated on an ITO glass substrate (sheet resistance = 20 Ω/sq) pre-cleaned in a sequence of anhydrous acetone, DI water, and methanol in an ultrasonic bath. The luminance area on the OLEDs was about 3 $mm^2 \times 3$ mm^2. After layer deposition the nanocomposite resin was dispensed on the ITO substrate and a glass lid was attached on to accomplish the OLED sample with a downward pressure about 0.5 kgf as schematically illustrated in Fig. 2. After the sealing, the OLED samples were sent to a UV oven and the curing was carried out at 80 °C in the wavelengths ranging from 280 nm to 400 nm for 24 min. The apparatus for the lifetime measurement of OLEDs consisted of a Photo Research PR50 spectrophotometer in conjunction to a Keithley 2400 source meter. A constant current attachment and photodiode arrays were adopted to monitor the luminance change of OLEDs as a function of time. This system was linked to a LabVIEW program for data acquisition/recording.

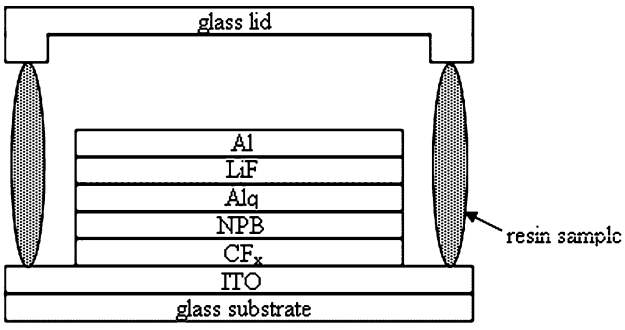

Fig. 2 Schematic representation of the OLED structure

Results and discussion

Crosslinking of acrylate and epoxy portions via photo-polymerization

Figures 3 and 4, respectively, present FTIR spectra and conversion ratios of resins samples UV-cured in air. No phase separation was observed in all specimens after UV-curing. During UV irradiation, the cationic photo-initiators were decomposed to generate free radicals and protonic acids to initiate the ring-opening process of epoxides while the radical photo-initiators produced free radicals to break C = C double bonds in acrylate groups. The amount of epoxide and acrylate groups hence decreased after UV exposure.

The conversion ratio was defined the degree of conversion of designated functional group in the resin sample subjected to UV irradiation:

$$\text{Conversion ratio}\,(\%) = \left(1 - \frac{\text{FTIR absorbance of functional group after UVcuring}}{\text{FTIR absorbance of functional group before UVcuring}}\right) \times 100$$

The band of oxirane ring in O_C at 795 cm^{-1} [12], C=C double bonds in acrylate groups at about 1410 cm^{-1} [12] and that in methylacrylate groups of the self-synthesized surfactants at about 1630 cm^{-1} [11] were adopted for conversion ratio calculation while the –C–H band of benzene in the specimens subjected UV curing was the reference absorbance of FTIR spectra.

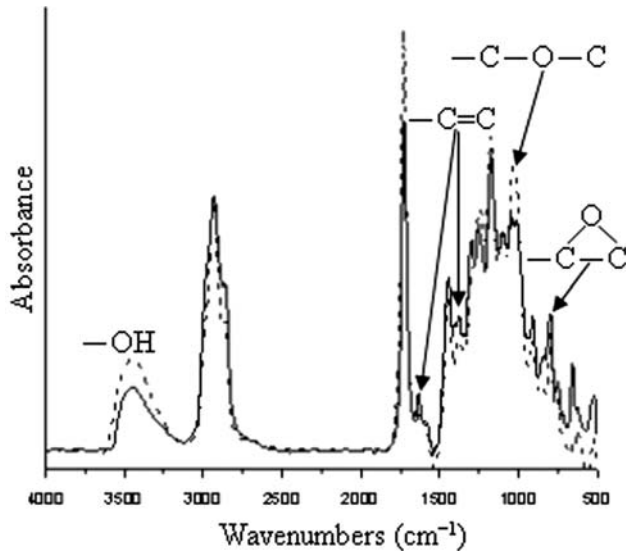

Fig. 3 FTIR spectra for (—) before-curing and (- - -) after-curing of: $S_{1\text{-RPI}}$

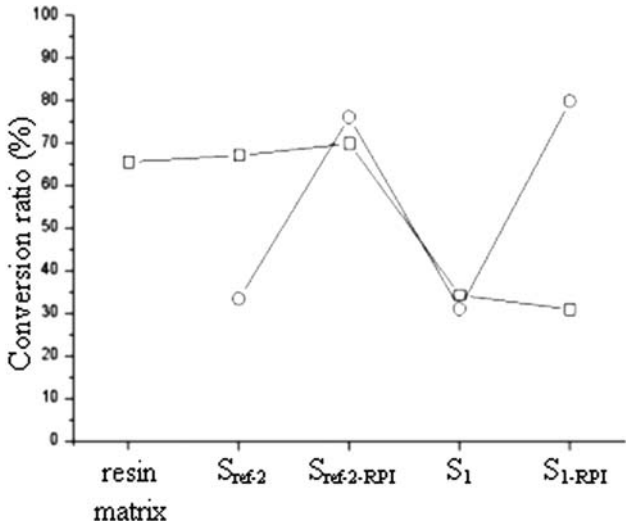

Fig. 4 Conversion ratio of: (□) for epoxide and (○) for C=C double bonds in resin samples

Further, the conversion ratio of C=C double bonds is an average of acrylate and methylacrylate groups in resin samples due to the similar polymerization mechanism. The conversion ratio of epoxides in resin matrix is about 66%. With the incorporation of M_I and M_{II}, the conversion ratio of epoxides in S_{ref-2} is approximately equal to 67% while that of C=C double bonds in S_{ref-2} is about 33%. The addition of radical photo-initiators increased the conversion ratio of C=C double bonds from 33% in S_{ref-2} to 76% in $S_{ref-2-RPI}$. When the photo-polymerization of acrylate/epoxide systems was carried out in air, moisture might serve as the catalyst in ring-opening polymerization to produce hydroxyl groups as the ending and O_2 tended to inhibit the radical-induced polymerization [12]. The conversion ratio of epoxides was thus higher than that of C=C double bonds. Although the conversion ratio of C=C double bonds was restricted, the radical photo-initiators enhanced the –(C–C)– bonds formation so as to promote the crosslinking density between M_I and M_{II}. In composite samples S_1 and S_{1-RPI}, the conversion ratios of epoxides drastically decreased to 34% and 31%, respectively. Further, the conversion ratio of C=C double bonds was activated by radical photo-initiators from 31% of S_1 to 80% of S_{1-RPI}. Similar reduction of conversion ratio in epoxides was also reported by Sui et al. [13]. As described above, [4-[(2-hydroxytetradecyl)oxy]phenyl]phenyliodonium hexafluoroantimonate were photo-decomposed into SbF_6^- and other segments. The SbF_6^- anions then attacked the hydrogen to form $HSbF_6$ for subsequent ring-opening process of epoxides. Due to the attachment of ionized 3°-N^+s in surfactants to acrylateclays, it was believed that SbF_6^- would be attracted by surfactants so as to restrain the generation of $HSbF_6$. The conversion ratios of epoxides in S_1/S_{1-RPI} therefore decreased in comparison with $S_{ref-2}/S_{ref-2-RPI}$.

The TGA data obtained in air were transformed into the DTG curves shown in Fig. 5 in order to analyze the bonding status of functional components in the resin samples [11, 14–16]. The DTG plot of resin matrix exhibits one major peak at about 380 °C and two minor peaks, respectively, at 505 °C and 550 °C. These three broad peaks represent different epoxy network areas formed by the ring-opening process of oxirane rings in O_C. When M_I containing three acrylate groups was added into the resin matrix, the radicals derived from photo-decomposition of cationic photo-initiators induced the radical photo-polymerization between acrylate groups so that a new peak around 340 °C was generated in the plot for S_{ref-1}. This implies a development of acrylate-based network structure by the formation of –(C–C)– bonds. An interpenetrating polymer network (IPN) structure formed by a synchronous photo-polymerization in acrylate-based/epoxide system [12] would therefore be formed in S_{ref-1}. Further, shrinkage of DTG peak at around 340 °C for S_{ref-2} and the new peak for S_{ref-1} was observed. The peak shrinkage in S_{ref-2} DTG plot also manifested the bonding between acrylate in M_I and methylacrylate groups in M_{II} [11], and was referred to the combination of acrylate-based and epoxy network structure. Although the photo-polymerization reactivity of oxirane rings in O_C was higher to react with the same groups due to higher ring strain [17], the oxirane rings in O_C and M_{II} could bond to each other *via* ring-opening process. The M_{II} hence transformed the IPN structure in S_{ref-1} into a dual polymer network in S_{ref-2}. Because methylacrylate groups in surfactants of acrylateclays also photo-polymerized with acrylate

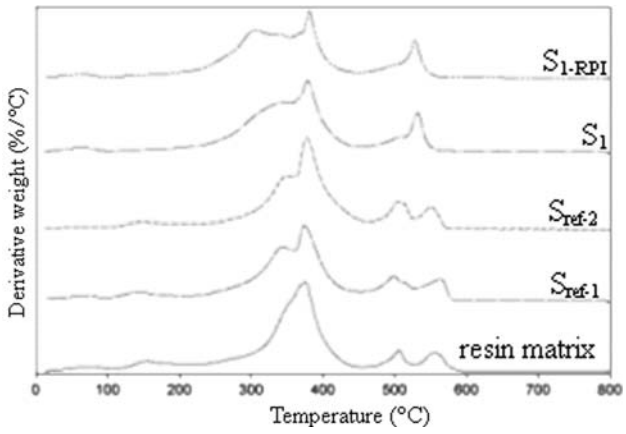

Fig. 5 DTG curves of resin samples in air ambient

groups in M_I, the peak corresponding to the thermal decomposition of –(C–C)– bonds broadened in S_1. The peak at about 340 °C in DTG plot of $S_{1\text{-RPI}}$ shifts to lower temperatures when the radical photo-initiator was added. As described in conversion ratio analysis the radical photo-initiators promoted the connection between acrylate and methylacrylate groups so that more thermally unstable –(C–C)– bonds were produced and the peak position varied. Above analyses clearly evidence that M_{II} effectively connected the acrylate-based and epoxy networks and generated a change in network structure during UV irradiation. The formation of –(C–C)– bonds between M_I/M_{II}/surfactants in the composite resin samples was also implied.

Microstructure of composite resin

Figure 6(a) and (b) depict the XRD patterns of acrylateclays and UV-cured nanocomposite resin samples. As revealed by the XRD pattern of acrylateclays, the self-synthesized surfactants synthesized in previous work effectively enlarges the galleries of clays from 1.36 nm of pristine MMT to 3.32 nm of acrylateclays [11]. After blending acrylateclays into $S_{ref\text{-}2}$ and $S_{ref\text{-}2\text{-}RPI}$ no distinct peak was observed in the XRD patterns of samples S_1 and $S_{1\text{-RPI}}$ as shown in Fig. 6(a); however, the grazing incidence X-ray measurement exhibits three peaks (see Fig. 6(b)) corresponding to a spatial periodicity of 4.83 nm. As shown in Fig. 7, the TEM microstructure characterization of $S_{1\text{-RPI}}$ revealed mixed exfoliated/intercalated morphology of clay in polymer matrix. Figure 7(a) depicts the dispersion of intercalated clay domains about 100 nm thick in the matrix and Fig. 7(b) shows the exfoliated lamellae about 1 nm thick in those domains. The *d*-spacing increment from 3.32 nm of acrylateclays to 4.83 nm of $S_{1\text{-RPI}}$ was attributed to the incorporation of M_I, M_{II} and O_C. The explanation of gallery enlargement and fine dispersion of inorganic clay in resin samples in terms of the compatibility of solubility parameters is given below.

The solubility parameter (δ), which is widely adopted to correlate the solute-solvent interactions, can be expressed as follows:

$$\delta = \sqrt{\frac{\sum E_{coh}}{\sum V}} \qquad (\text{unit: } \sqrt{\text{J/cm}^3})$$

where E_{coh} is the cohesive energy and V is the molar volume of functional parts of single molecule. Further, the dispersion of solute in solvent could be distinguished by the differential of solubility parameters between solute and solvent. There is good compatibility between solute and solvent when the difference of solubility parameters is less than 1. In this study, similar solubility parameters between acetone (calculated value = 18.55) and λ-shaped surfactant (calculated value = 19.43) indicate that acetone is compatible with surfactants in acrylateclays and may easily penetrate into lamellar structure during swelling. When acetone was removed from swollen acrylateclays, the M_I molecules entered into the acrylateclay galleries instead of surrounding the acrylateclays due to the small difference of solubility parameters between surfactants and M_I (calculated value = 20.22). When M_{II} (calculated value = 20.93) was sequentially added into acrylateclays/M_I mixture, the small difference of solubility parameters between M_I, M_{II} and O_c (calculated value = 20.75) further implied a fine dispersion of acrylateclays in resin matrix. According to calculated solubility parameters cited above, before UV curing fine dispersion of acrylateclay domains in resin matrix was achieved with the presence of small amounts of M_I and M_{II}. During UV irradiation, M_I served as a hub providing multiple sites to link acrylateclays and M_{II} by forming –(C–C)– bonds, while M_{II} acted as ''connectors'' between acrylate-based and epoxide networks as evidenced by previous DTG analyses. After UV curing, the *d*-spacing enlargement

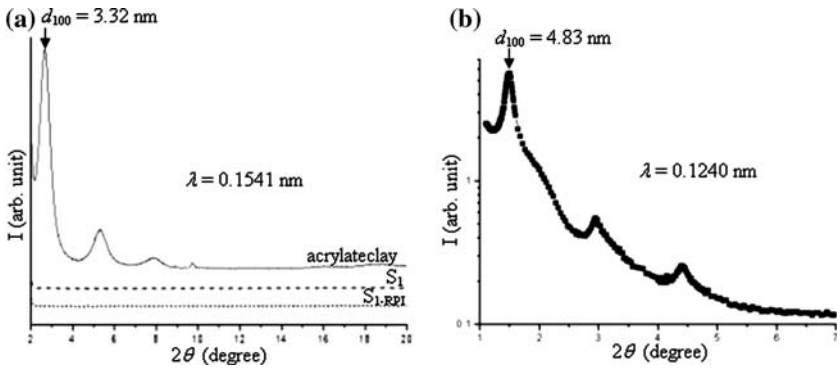

Fig. 6 (**a**) XRD patterns of acrylateclays, S_1 and $S_{1\text{-RPI}}$ and (**b**) GIXRD pattern of $S_{1\text{-RPI}}$ with incident angle fixed at 0.25°

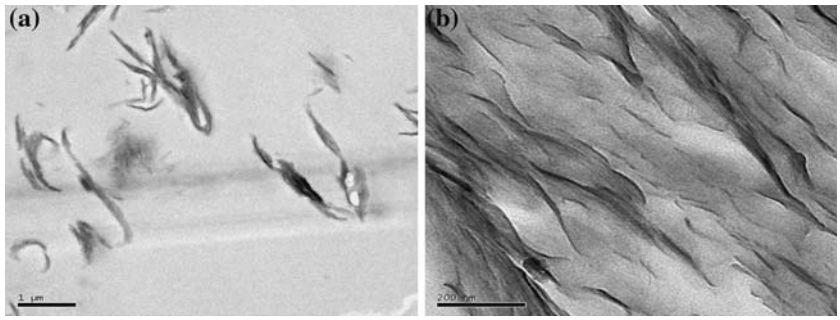

Fig. 7 (**a**) TEM micrograph of $S_{1\text{-RPI}}$ and (**b**) enlargement of portion in (**a**)

of inorganic clays from 3.32 nm to 4.83 nm evidenced that additive monomers indeed enter the clay galleries due to the similar solubility parameters and subsequent crosslinking between surfactants/M_I/M_{II} occurs as identified by DTG analysis. The intercalated acrylate-clay domains in conjunction with exfoliated lamellae structure in the composite resin samples thus formed. Another evidence for the fine dispersion of clay lamellae is the low conversion ratio of epoxides in O_C resulted from the attachment of surfactants onto the clay platelets although distinct difference of solubility parameters predicts the separation of O_C from surfactants in nanocomposite samples.

Thermal properties

Table 3 presents the thermal resistance and inorganic content of epoxide/acrylateclays nanocomposite resins prepared in this work. The TMA curves of resin samples measured in nitrogen ambient are given in Fig. 8. The inorganic contents listed in Table 3 indicate that the clay contents in S_1 and $S_{1\text{-RPI}}$ are about 4.8 wt.% and 4.6 wt.%, respectively, *via* TGA measurement in air ambient. As reported previously [11], acrylateclays consisted of approximate 42.7 wt.% λ-shaped surfactants for galleries enlargement and 57.3 wt.% of MMT. Since the ratio of the resin matrix/M_I/M_{II} mixture to acrylateclays was 9:1, the maximum amount of inorganic clays remained in nanocomposite samples would be 5.73 wt.%. The thermal analysis hence found about 5 wt.% of clay content in samples S_1/$S_{1\text{-RPI}}$.

The temperature corresponding to 5% weight loss ($T_{d\text{-}5\%}$) of resin matrix in nitrogen ambient is about 149°C, and $T_{d\text{-}5\%}$ of $S_{\text{ref-}2}$ increased to 170 °C. When 5 wt.% of inorganic clays was added in $S_{\text{ref-}2}$, the $T_{d\text{-}5\%}$ of the sample S_1 raised to about 198 °C and the addition of radical photo-initiators in S_1 further increased the $T_{d\text{-}5\%}$ of sample $S_{1\text{-RPI}}$ to 213 °C. In addition to the $T_{d\text{-}5\%}$'s representing the thermal resistance of nanocomposite resins, $T_{d\text{-}10\%}$ and $T_{d\text{-}20\%}$ are also adopted to explain the crosslinking status in nanocomposite samples. According to Table 3, it is found that the existence of M_I/M_{II} in $S_{\text{ref-}2}$ benefits the thermal resistance due to the increments from 208 °C to 268 °C for $T_{d\text{-}10\%}$ and 304 °C to 334 °C for $T_{d\text{-}20\%}$; nevertheless, $T_{d\text{-}10\%}$ and $T_{d\text{-}20\%}$ of S_1 are less than those of $S_{\text{ref-}2}$. The radical photo-initiators in $S_{1\text{-RPI}}$ increased $T_{d\text{-}10\%}$ and $T_{d\text{-}20\%}$ of S_1 from 256 °C to 279 °C and 299 °C to 321 °C, respectively. In the beginning of heating, the new dual networks in $S_{\text{ref-}2}$ formed by –(C–C)– bonds between M_I/M_{II} and –(C–O–C)– bonds between M_{II}/O_C provide a better thermal resistant. Furthermore, high thermal resistance of clays, the chemical bonds between surfactants/resin matrix [18–21] and the conformational hindrance derived from exfoliated clay nanostructure identified in microstructure analysis, which retards the diffusion of decomposed segments

Table 3 Thermal properties of resin samples

	Residual weight (%)	$T^a_{d\text{-}5\%}$ (°C)	$T^a_{d\text{-}10\%}$ (°C)	$T^a_{d\text{-}20\%}$ (°C)
Resin matrix	–	149 ± 4	208 ± 6	304 ± 7
$S_{\text{ref-}2}$	–	170 ± 6	268 ± 7	334 ± 7
S_1	4.8 ± 0.2	198 ± 5	256 ± 7	299 ± 8
$S_{1\text{-RPI}}$	4.6 ± 0.1	213 ± 6	279 ± 6	321 ± 7

[a] $T_{d\text{-}x\%}$ is the temperature at which the resin samples lost x% in weight. For example, $T_{d\text{-}20\%}$ = 334 °C means the temperature at which $S_{\text{ref-}2}$ lost 20% of its original weight

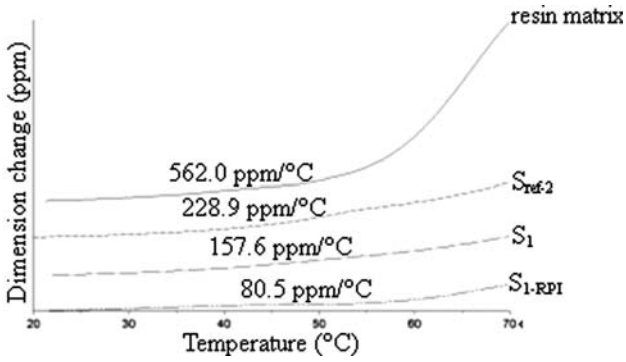

Fig. 8 TMA curves of resin samples in nitrogen ambient

during heating [22], implied higher $T_{d\text{-}5\%}$'s of nanocomposite samples. In other words, such a hindrance led to the confinement of photo-initiators diffusion and subsequent constraint of network growth [23]. It limited the crosslinking of M_I and M_{II} near exfoliated lamellae so that small network structure between lamellae formed. These small networks caused early thermal degradation [24] and hence lower $T_{d\text{-}10\%}$ and $T_{d\text{-}20\%}$ of S_1. The addition of radical photo-initiators increased the amount of small networks by crosslinking the dispersed acrylate-based groups, even enhanced the growth of such networks between galleries so that further improvement of thermal resistance was observed.

As given in Fig. 8, the small amount of additive monomers effectively decreased the CTE from 562.0 ppm/°C of resin matrix to 228.9 ppm/°C of $S_{ref\text{-}2}$. Adding the acrylateclays into $S_{ref\text{-}2}$ also reduced the CTE to 157.6 ppm/°C for S_1. Furthermore, the CTE of the nanocomposite resin $S_{1\text{-}RPI}$ diminished to 80.5 ppm/°C when the radical photo-initiators were added in S_1. A dual polymer network structure is more rigid in comparison with the pure epoxy network structure so that substantially improvement of CTE could be speculated. The $S_{ref\text{-}2}$ with such a compact structure consequently exhibited a lower CTE by the crosslinking between M_I, M_{II} and O_C. In addition, it is known that the inorganic clays with low CTE characteristic also reduce the CTE of nanocomposites. The relatively low CTE of $S_{1\text{-}RPI}$ was hence attributed to the addition of acrylateclays and the increase of crosslinking between components in polymeric matrix and surfactants in acrylateclays.

Optical properties

Transmittances of resin matrix and two relevant nanocomposite resin samples are shown in Fig. 9. In general, the transmittance of composites in the visible light region decreases due to the addition of opaque clays; however, the fine dispersion and well exfoliation of clay lamellae would not deteriorate the transmittance of nanocomposite resins prepared in this work. As shown in Fig. 9, there is no drastic change of transmittance between resin matrix and nanocomposite resin samples and the calculation indicated the average transmittance changes from 86% to 85% when 5 wt.% of inorganic filler was added. The transmittance slightly dropped to 83% when radical photo-initiators were further added into the nanocomposite specimens. Because the sizes of intercalated clay domains and exfoliated lamellae were much smaller than the wavelength of visible light, the nanocomposite resin hence retained good transparency after hybridization.

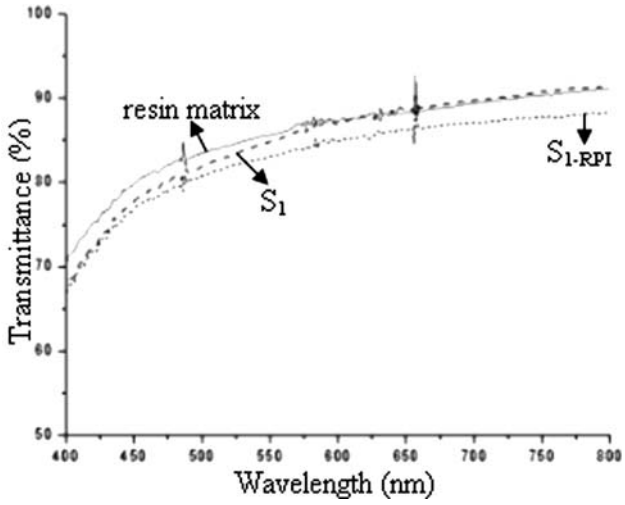

Fig. 9 Optical transmittance of resin samples. The thickness of resin samples was about 100 μm

Adhesion strength and moisture absorption

Table 4 presents the moisture absorption and adhesion strength on glass substrate of samples. The moisture absorption was obtained by calculating the weight ratio of H_2O absorption in nanocomposite samples before and after immersing in the water. The moisture absorption decreased from 12.7% for resin matrix to 8.5% for $S_{ref\text{-}2}$. After the addition of acrylateclays into polymeric portions, the moisture absorption further reduced to 7.3% for S_1 and 6.1% for $S_{1\text{-}RPI}$. Meanwhile, the adhesion strength of resin matrix decreased from 59.1 kgf/cm^2 to 50.4 kgf/cm^2 when specific amounts of M_I and M_{II} were added. The addition of acrylateclays and radical photo-initiators decreased the adhesion strength to moderate values: 45.7 kgf/cm^2 for S_1 and 43.8 kgf/cm^2 for $S_{1\text{-}RPI}$. Owing to the hydroxyl groups at the end of epoxy networks, it is believed that the acrylate-based groups possess higher resistance to moisture permeation and inferior adhesion property in comparison with epoxy groups. Hence according to the

Table 4 Moisture absorption and adhesion strength of resin samples

	Moisture absorption (%)	Adhesion strength (kgf/cm^2)
Resin matrix	12.7 ± 0.5	59.1 ± 2.2
$S_{ref\text{-}2}$	8.5 ± 0.6	50.4 ± 2.1
S_1	7.3 ± 0.6	45.7 ± 2.3
$S_{1\text{-}RPI}$	6.1 ± 0.7	43.8 ± 2.4

conversion ratio analysis, $S_{ref\text{-}2}$ was expected to exhibit lower moisture absorption and adhesion strength when acrylate-based portions were interlaced in epoxy networks. Furthermore, the long diffusion length derived from the large aspect ratio of clay lamellae also retarded the moisture permeation so that the intercalated/exfoliated nanocomposite resin samples prepared in this work possessed lower moisture absorption. Meanwhile, small networks resulted from the chemical bonding between $S_{ref\text{-}2}$ and surfactants in acrylateclays not only promoted the exfoliation of clay lamellae into nanometer scale but also increased the compatibility between polymeric portions and inorganic fillers. Though deterioration of adhesion property was expected with the addition of acrylate-based networks and inorganic filler, there is no drastic decrease of adhesion strength for nanocomposite resins prepared in this work.

Lifetimes of sealed OLEDs

Figure 10 shows the lifetimes of OLEDs sealed by different resin samples. In this work the lifetime was defined as the time span for normalized luminance of the device drops to 50% (t_{50}). As shown in Fig. 10 the lifetime of the $S_{ref\text{-}2\text{-}RPI}$-sealed OLED is near 150 h while that of the $S_{1\text{-}RPI}$-sealed OLED is about 300 h. In this part of study, since the degradation phenomena related to the self-deterioration of light-emitting layer (EML), material interdiffusion and oxidation of cathode metal were not observed, the moisture/oxygen attacks were hence considered as the root cause of luminance decline of OLEDs [25]. The improved lifetime of $S_{1\text{-}RPI}$-sealed OLED indicates that the well dispersed intercalated clay domains and exfoliated clay platelets in polymeric matrix implied the long diffusion length for the permeation of moisture and oxygen molecules [26]. Since their migration was effectively retarded, better lifetime property of OLEDs sealed by nanocomposite resins was hence achieved.

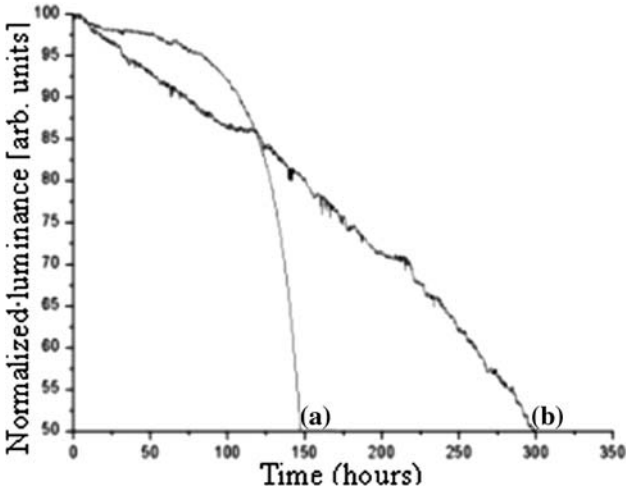

Fig. 10 Normalized luminance of OLEDs sealed in air by using (**a**) $S_{ref\text{-}2\text{-}RPI}$ and (**b**) $S_{1\text{-}RPI}$

Conclusions

This work demonstrates the preparation of UV-curable intercalated/exfoliated nanocomposite resin by the combination of acrylateclays and epoxy resin *via* the addition of functional monomers, M_I and M_{II}, under the consideration of solubility compatibility and chemical reactivity. Due to the good compatibility of M_I, M_{II} and cationic oligomer with surfactants in acrylateclays, a fine dispersion of acrylateclay domains in polymeric matrix was achieved. As revealed by conversion ratio and DTG analyses, the conversion ratio of epoxides in O_C was affected by the ionized 3°-N^+s in the surfactant of nanocomposite specimens; further, the –(C–C)– and –(C–O–C)– bonds both generated during UV irradiation and it depicted the formation of chemical bonds between resin matrix/acrylateclays/M_I/M_{II}. A hybrid acrylate-based/epoxy network originated from the photo-crosslinking between acrylateclays, monomers and oligomers were therefore formed. The interactions further intensified the *d*-spacing enlargement of clay lamellae that, as evidenced by XRD and TEM characterizations, the nanocomposite resins indeed contained intercalated clay domains with exfoliated lamellae. Thermal analyses revealed that the existence of exfoliated clays structure effectively increases the $T_{d\text{-}5\%}$ and the crosslinking between acrylateclays and polymeric matrix hence lowers the CTE of nanocomposite resins. However, the hindrance for exfoliated lamellae might limit the network growth and such an influence was observed in the characterization of $T_{d\text{-}10\%}$ and $T_{d\text{-}20\%}$ of samples. The fine dispersion of clay domains and lamellae in polymeric matrix also decreased the moisture absorption without deteriorating the transparency of resins samples. Though addition of acrylate-based monomers and inorganic clay fillers was expected to reduce the adhesion strength of nanocomposite resin, satisfactory adhesion property was obtained due to the nanometer-scale dispersion of the exfoliated clay lamellae and good compatibility between polymeric matrix and acrylateclays. The UV-curable nanocomposite resins prepared in this work were subsequently applied to the OLED packaging. A better lifetime of OLEDs was obtained due to the improved physical properties of nanocomposite resins reported above.

Acknowledgements This work was supported by the Ministry of Education, Taiwan, Republic of China within the Project of Excellence ''Semiconducting Polymers and Organic Molecules for Electroluminescence: B. Development of Advanced Materials and Devices for Organic Light Emitting Diodes (OLED) Technology'' under contract No. 91-E-FA04-2-4. The authors are also grateful to Dr. Chia-Hung Hsu at NSRRC, Taiwan, for the assistance and discussion on GIXRD measurements.

References

1. Nagata H, Shiroishi M, Miyama Y, Mitsugi N, Miyamoto N (1995) Opt Fib Tech 1:283
2. Baikerikar KK, Scranton AB (2001) Polym 42:431
3. Chou YC, Wang YY, Hsieh TE, J Appl Polym Sci (accepted)
4. Wang YY, Hsieh TE, IEEE Trans Adv Package (accepted)
5. Decker C, Zahouily K, Keller L, Benfarhi S, Bendaikha T (2002) J Mater Sci 37:4831
6. Keller L, Decker C, Zahouily K, Benfarhi S, Le Meins JM, Miehe-Brendle J (2004) Polym 45:7437
7. Shemper BS, Morizur JF, Alirol M, Domenech A, Hulin V, Mathias LJ (2004) J Appl Polym Sci 93:1252
8. Benfarhi S, Decker C, Keller L, Zahouily K (2004) Eur Polym J 40:493
9. Uhl FM, Davuluri SP, Wong SC, Webster DC (2004) Polym 45:6175
10. Wang YY, Hsieh TE (2005) Chem Mater 17:3331
11. Chiang TH, Hsieh TE (2005) J Adhes Sci Tech 1:1
12. Decker C, Nguyen Thi Viet T, Decker D, Weber-Koehl E (2001) Polym 42:5531
13. Sui G, Zhang ZG, Chen CQ, Zhong WH (2002) Mater Chem Phys 78:349
14. Jana RN, Mukunda PG, Nando GB (2003) Polym Degrad Stab 80:75
15. Remiro PM, Cortazar M, Calahorra E, Calafel MM (2002) Polym Degrad Stab 78:83
16. Basfer AA (2002) Polym Degrad Stab 77:221
17. Crivello JV, Varlemann U (1995) J Polym Sci 33:2473
18. Wen J, Wikes GL (1996) Chem Mater 8:1667
19. Fischer HR, Gielgens LH, Koster TPM (1999) Acta Polym 50:122
20. Petrović ZS, Javni I, Waddon A, Bánhegyi G (2000) J Appl Polym Sci 76:133
21. Zhu ZK, Yang Y, Yin J, Wang XY, Ke YC, Qi ZN (1999) J Appl Polym Sci 73:2063
22. Burnside SD, Giannelis EP (1995) Chem Mater 7:1597
23. Fu X, Qutubuddin S (2001) Polym 42:807
24. Lee DK, Char KK (2002) Polym Degrad Stab 75:555
25. Laubender J, Chkoda L, Sokolowski M, Umbach E (2000) Synth Met 111–112:373
26. Yano K, Usuki A, Okada A, Kurauchi T, Kamigatio O (1993) J Polym Sci A Polym Chem 31:2493